CHEMISTRY OF MATERIALS
Article

*Chem. Mater.* **2011,** *23,* 39–47 39
DOI:10.1021/cm1025427

# $^{71}$Ga Slow-CTMAS NMR and Crystal Structures of MOF-Type Gallium Carboxylates with Infinite Edge-Sharing Octahedra Chains (MIL-120 and MIL-124)

Redouane Hajjar,[†] Christophe Volkringer,[‡,⊥] Thierry Loiseau,*[,‡,⊥] Nathalie Guillou,[‡] Jérôme Marrot,[‡] Gérard Férey,[‡] Irene Margiolaki,[§] Gerhard Fink,[†] Claudia Morais,[†,¶] and Francis Taulelle[†]

[†]*Institut Lavoisier* (*UMR CNRS 8180*), *and* [‡]*Porous Solids Group & Tectospin Group, Université de Versailles Saint Quentin en Yvelines, 45, avenue des Etats-Unis, 78035 Versailles, and* [§]*ESRF, 6 rue Jules Horowitz, B.P. 220, 38043 Grenoble cedex, France.* [⊥]*Current address: Unité de Catalyse et Chimie du Solide* (*UCCS*), *UMR CNRS 8181, Université de Lille Nord de France, USTL-ENSCL, 59652 Villeneuve d'Ascq, France.* [¶]*Current address: Laboratoire de Catalyse en Chimie Organique* (*LACCO*), *UMR CNRS 6503, Université de Poitiers, 86022 Poitiers cedex, France.*

*Received September 6, 2010. Revised Manuscript Received November 22, 2010*

Two gallium carboxylates of MOF-type have been hydrothermally synthesized (210 °C) by using 1,2,4,5-benzenetetracarboxylate ($Ga_4(OH)_8[C_{10}O_8H_2]\cdot 5-5.6H_2O$ or MIL-120) or 1,2,4-benzenetricarboxylate ($Ga_2(OH)_4[C_9O_6H_4]$ or MIL-124) as linkers. The structures of both compounds solved from XRD analysis, revealed two independent crystallographic sites for the gallium atoms, which are connected to each other through $\mu_2$-hydroxo edge, generating zigzag chains with a cis−trans mode. The inorganic ribbons are linked to each other via all the carboxylate functions of the pyromellitate ligand to form a 3D framework (MIL-120) or two of the carboxylate arms of the trimellitate ligand to form a 2D structure (MIL-124). For the latter, one of the carboxylate arms is not bonded to the gallium centers, resulting in the layered aspect of the final structure. Solid-state NMR using the slow-CTMAS method has been successfully implemented for the determination of the gallium site parameters for MIL-120, allowing more resolved spectra at moderate magnetic fileds than at very high field. Only one gallium site is visible for MIL-124, indicating a dynamic disorder resulting from the nonfully connected carboxylate species of the trimellitate ligand.

## Introduction

The interest in the field of porous crystalline metal−organic frameworks (MOF) is growing exponentially for the last decades. These hybrid materials, which combine inorganic motifs together with organic linkers (N-donor or O-donor such as carboxylate function) exhibit fascinating porous networks with systems of multidimensional crossing channels and/or extra-large cavities of several nanometers size. Many applications such as molecule adsorption and separation, drug delivery, catalysis, are now considered for this emerging class of compounds.[1−9] Regarding the inorganic part, most of the metallic cations belong to the class of the transition metals of the first raw of the periodic table, but others such as trivalent elements of the block IIIA column or lanthanides have also been employed. Among them, the use of gallium was not reported very often in literature despite that it could be a good candidate for the elaboration of such MOF type architectures. It is recently involved in the formation of large "gallic" wheel arrangements[10−12] containing $Ga_{10}$, $Ga_{18}$, or $Ga_{20}$ centers, stabilized by carboxylates molecules for instance. Other molecular motifs were also isolated with different nuclearities.[13−17] However extended gallium-based networks have been isolated with different polytopic carboxylate

*To whom correspondence should be addressed. E-mail: thierry.loiseau@ensc-lille.fr. Phone: (33) 3 20 434 434. Fax: (33) 3 20 436 814.

(1) Férey, G. *Chem. Soc. Rev.* **2008**, *37*, 191.
(2) Yaghi, O. M.; O'Keeffe, M.; Ockwig, N. W.; Chae, H. K.; Eddaoudi, M.; Kim, J. *Nature* **2003**, *423*, 705.
(3) Kitagawa, S.; Kitaura, R.; Noro, S.-I. *Angew. Chem., Int. Ed.* **2004**, *43*, 2334.
(4) Czaja, A. U.; Trukhan, N.; Müller, U. *Chem. Soc. Rev.* **2009**, *38*, 1203.
(5) Ma, L.; Abney, C.; Lin, W. *Chem. Soc. Rev.* **2009**, *38*, 1248.
(6) Murray, L. J.; Dinca, M.; Long, J. R. *Chem. Soc. Rev.* **2009**, *38*, 1294.
(7) Lee, J. Y.; Farha, O. K.; Rioberts, J.; Scheidt, K. A.; Nguyen, S. B. T.; Hupp, J. T. *Chem. Soc. Rev.* **2009**, *38*, 1450.
(8) Li, J.-R.; Kuppler, R. J.; Zhou, H.-C. *Chem. Soc. Rev.* **2009**, *38*, 1477.
(9) Horcajada, P.; Chalati, T.; Serre, C.; Gillet, B.; Sebrie, C.; Baati, T.; Eubank, J. F.; Heurtaux, D.; Clayette, P.; Kreuz, C.; Chang, J.-S.; Hwang, Y. K.; Marsaud, V.; Bories, P.-N.; Cynober, L.; Gil, S.; Férey, G.; Couvreur, P.; Gref, R. *Nat. Mater.* **2010**, *9*, 172.
(10) King, P.; Stamatatos, T. C.; Abboud, K. A.; Christou, G. *Angew. Chem., Int. Ed.* **2006**, *45*, 7379.
(11) Stamatatos, T. C.; Mukherjee, S.; Abboud, K. A.; Christou, G. Chem. Commun. **2009**.
(12) Cheng, C.-Y.; Stamatatos, T. C.; Christou, G.; Bowers, C. R. *J. Am. Chem. Soc.* **2010**, *132*, 5387.
(13) Bulc, N.; Golic, L.; Siftar, J. *Acta Crystallogr. C* **1984**, *40*, 1829.
(14) Andras, M. T.; Duraj, S. A.; Hepp, A. F.; Fanwick, P. E.; Bodnar, M. M. *J. Am. Chem. Soc.* **1992**, *114*, 786.
(15) O'Brien, P.; Salacinski, H.; Motevalli, M. *J. Am. Chem. Soc.* **1997**, *119*, 12695.


Published on Web 12/13/2010

ligands, such as terephthalate (MIL-53,[18−20] MIL-68[21]), trimesate (MIL-96[22]), acetate,[23] pyromellitate (MIL-61[24]), or naphthalenetetracarboxylate (MIL-122[25]). Most of them are isostructural with the parent *p* block elements aluminum[25−27] or indium,[21,23,25,28−30] or other trivalent transition metals such as vanadium,[31,32] chromium,[33] or iron.[34]

We have continued our investigations in the gallium system with different aromatic multicarboxylate ligands. In this context, we found a series of compounds with structures built up from similar inorganic motif consisting of uncommon edge-sharing $GaO_6$ octahedra generating infinite chains. This type of building block was previously described in the aluminum pyromellitate MIL-120[35] (pyromellitate: 1,2,4,5-benzenetetracarboxylate; MIL stands for Materials of 'Institut Lavoisier') and we succeeded in the isolation of the gallium isotype, $Ga_4(OH)_8[C_{10}O_8H_2]\cdot 5-5.6H_2O$. A second solid with such an inorganic motif was also stabilized with the trimellitate linker (1,2,4-benzenetricarboxylate) in a compound $Ga_2(OH)_4[C_9O_6H_4]$), hereafter called MIL-124.

This contribution deals with the hydrothermal synthesis of these two gallium-based MOF compounds, MIL-120 and MIL-124. Their structural studies have been performed by combining several analysis techniques, including: powder and single-crystal X-ray diffraction, thermogravimetry, infrared spectroscopy and solid-state NMR (SSNMR) spectroscopy. The NMR study of quadrupolar nuclei such as $^{71}Ga$ is now carried out with high magnetic fields by using either nonroutine or routine experiments, such as: QPASS,[36] MQMAS,[37,38] and STMAS,[39] which can provide high resolution spectra. The cost of this resolution is the use of high radio frequency (RF) fields, fast magic angle spinning (MAS) speed and small spectral width. High resolution can be also obtained at moderate magnetic field and by applying soft RF and slow MAS speed, as proposed by Persons and Harbison,[40] a solution, christened as STREAQI, that has not been reported after its initial discovery. This method is based on the use of a selective quadrupolar echo and correlates the central transitions to itself using slow MAS speed. In order to bring this experiment into the family of high resolution quadrupolar 2D NMR measurement, the acronym has been substituted from STREAQI to slow-CTMAS to show of its similar properties with MQMAS and STMAS. In this work we took the opportunity to choose this second approach applied to gallium-based MOF type materials, and simplified the line shape analysis to extract the quadrupolar parameters.

## Experimental Section

**Synthesis.** Both MIL-120 and MIL-124 compounds have been hydrothermally synthesized under autogenous pressure. The starting reactants are gallium nitrate ($Ga(NO_3)_3\cdot xH_2O$, Alfa Aesar, 99.9%), 1,2,4,5-benzenetetracarboxylic acid, (noted $H_4$btec, $C_6H_2(CO_2H)_4$, Aldrich, 96%), 1,2,4-benzenetricarboxylic acid (noted 1,2,4-$H_3$btc, $C_6H_3(CO_2H)_3$, Alfa Aesar, 99%), and deionized water and were used without further purification.

Typically, the MIL-120 (Ga) phase ($Ga_4(OH)_8[C_{10}O_8H_2]\cdot 5-5.6H_2O$) was obtained from a mixture of 0.3 g gallium nitrate (1.2 mmol), 0.05 g $H_4$btec (0.2 mml), and 5 mL $H_2O$ (277.7 mmol), placed in a 23 mL Teflon-lined stainlees steel autoclave (Parr), which is then heated at 210 °C for 2 h. The initial pH value was 1.0 and then decreased down to 0.7 after the hydrothermal treatment. The resulting powdered product was filtered off and washed with deionized water in reflux during 24 h and then dried at room temperature. MIL-120 (Ga) is identified as needle-like crystals of 20−40 $\mu$m length and 1−2 $\mu$m section (Figure 1) from the SEM examination (1530 LEO Gemini). The photograph clearly showed the specific crystal growth from a nucleation point, giving rise to the formation of cone-shaped aggregates of needles stacking. It was observed that longer reaction times induced the formation of another gallium pyromellitate MIL-61,[24] previously characterized in our group.

The second phase MIL-124 ($Ga_2(OH)_4[C_9O_6H_4]$) was synthesized from a mixture of 0.6 g gallium nitrate (2.4 mmol), 0.37 g 1,2,4-btc (1.8 mmol) and 5 mL $H_2O$ (277.8 mmol), which was heated at 210 °C for 24 h. The initial and final pH values were 0.4 and 0.6, respectively. The powdered solid was filtered off and washed with deionized water and dried at room temperature. SEM examination of the MIL-124 phase shows large platelet-shaped crystals of 100−250 $\mu$m length (Figure 1).

(16) Schmitt, W.; Anson, C. E.; Sessoli, R.; van Veen, M.; Powel, A. K. *J. Inorg. Biochem.* **2002**, *91*, 173.
(17) Goodwin, J. C.; Teat, S. J.; Heath, S. L. *Angew. Chem., Int. Ed.* **2004**, *43*, 4037.
(18) Vougo-Zanda, M.; Huang, J.; Anokhina, E.; Wang, X.; Jacobson, A. J. *Inorg. Chem.* **2008**, *47*, 11535.
(19) Volkringer, C.; Loiseau, T.; Guillou, N.; Férey, G.; Elkaim, E.; Vimont, A. *Dalton Trans.* **2009**, 2241.
(20) Chaplais, G.; Simon-Masseron, A.; Porcher, F.; Lecomte, C.; Bazer-Bachi, D.; Bats, N.; Patarin, J. *Phys. Chem. Chem. Phys.* **2009**, *11*, 5241.
(21) Volkringer, C.; Meddouri, M.; Loiseau, T.; Guillou, N.; Marrot, J.; Férey, G.; Haouas, M.; Taulelle, F.; Audebrand, N.; Latroche, M. *Inorg. Chem.* **2008**, *47*, 11892.
(22) Volkringer, C.; Loiseau, T.; Férey, G.; Morais, C.; Taulelle, F.; Montouillout, V.; Massiot, D. *Microporous Mesoporous Mater.* **2007**, *105*, 111.
(23) Mensinger, Z. L.; Zakharov, L. N.; Johnson, D. W. *Inorg. Chem.* **2009**, *48*, 3505.
(24) Loiseau, T.; Muguerra, H.; Haouas, M.; Taulelle, F.; Férey, G. *Solid State Sci.* **2005**, *7*, 603.
(25) Volkringer, C.; Loiseau, T.; Guillou, N.; Férey, G.; Elkaïm, E. *Solid State Sci.* **2009**, *11*, 1507.
(26) Loiseau, T.; Lecroq, L.; Volkringer, C.; Marrot, J.; Férey, G.; Haouas, M.; Taulelle, F.; Bourrely, S.; Llewellyn, P. L.; Latroche, M. *J. Am. Chem. Soc.* **2006**, *128*, 10223.
(27) Loiseau, T.; Serre, C.; Huguenard, C.; Fink, G.; Taulelle, F.; Henry, M.; Bataille, T.; Férey, G. *Chem.—Eur. J.* **2004**, *10*, 1373.
(28) Anokhina, E. V.; Vougo-Zanda, M.; Wang, X.; Jacobson, A. J. *J. Am. Chem. Soc.* **2005**, *127*, 15000.
(29) Volkringer, C.; Loiseau, T. *Mater. Res. Bull.* **2006**, *41*, 948.
(30) Lin, Z.-Z.; Jiang, F.-L.; Chen, L.; Yuan, D.-Q.; Zhou, Y.-F.; Hong, M.-C. *Eur. J. Inorg. Chem.* **2005**, 77.
(31) Barthelet, K.; Marrot, J.; Férey, G.; Riou, D. *Chem. Commun.* **2004**, 520.
(32) Barthelet, K.; Riou, D.; Nogues, M.; Férey, G. *Inorg. Chem.* **2003**, *42*, 1739.
(33) Serre, C.; Millange, F.; Thouvenot, C.; Nogues, M.; Marsolier, G.; Louër, D.; Férey, G. *J. Am. Chem. Soc.* **2002**, *124*, 13519.
(34) Whitfield, T. R.; Wang, X.; Liu, L.; Jacobson, A. J. *Solid State Sci.* **2005**, *7*, 1096.
(35) Volkringer, C.; Loiseau, T.; Haouas, M.; Taulelle, F.; Popov, D.; Burghammer, M.; Riekel, C.; Zlotea, C.; Cuevas, F.; Latroche, M.; Phanon, D.; Knöfelv, C.; Llewellyn, P. L.; Férey, G. *Chem. Mater.* **2009**, *21*, 5783.
(36) Massiot, D.; Montouillout, V.; Fayon, F.; Florian, P.; Bessada, C. *Chem. Phys. Lett.* **1997**, *272*, 295.
(37) Medek, A.; Harwood, J. S.; Frydman, L. *J. Am. Chem. Soc.* **1995**, *117*, 12779.
(38) Frydman, L.; Harwood, J. S. *J. Am. Chem. Soc.* **1995**, *117*, 5367.
(39) Gan, Z. *J. Am. Chem. Soc.* **2000**, *122*, 3242.
(40) Persons, J.; Harbison, G. S. *J. Magn. Reson.* **2007**, *186*, 347.

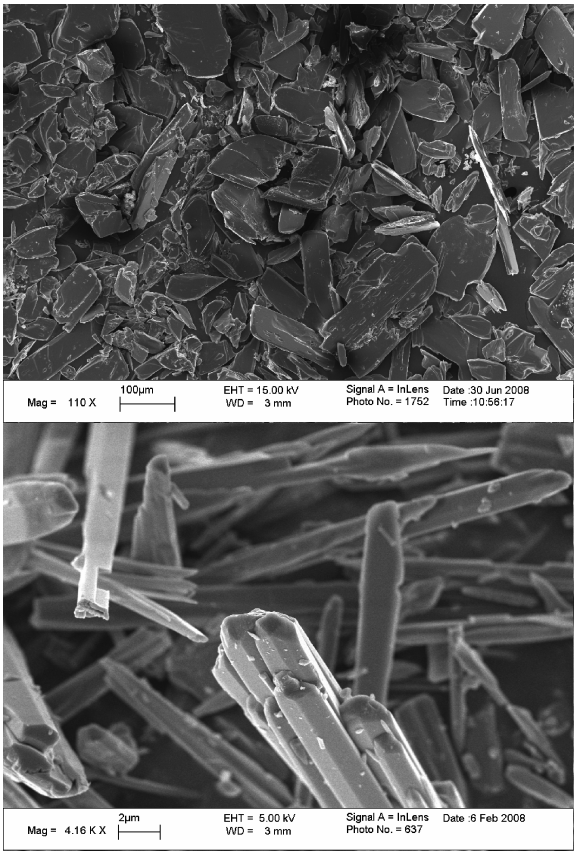


**Figure 1.** SEM images of the gallium trimellitate MIL-124 (top) and the gallium pyromellitate MIL-120 (bottom).

**Single-Crystal XRD Analysis.** A colorless platelet-like crystal of MIL-124 (220 × 100 × 20 $\mu$m) was selected and glued by Araldite to a tapered glass fiber under an optical microscope. X-ray intensity data were collected on a Bruker X8-APEX2 CCD area-detector diffractometer using Mo $K_\alpha$ radiation ($\lambda$ = 0.71073 Å). Four sets of narrow data frames (60 s per frame) were collected at different values of $\theta$ for 2 and 2 initial values of $\phi$ and $\omega$, respectively, using 0.3° increments of $\phi$ or $\omega$. Data reduction was accomplished using SAINT, version 7.03. The substantial redundancy in data allowed a semiempirical absorption correction (SADABS, version 2.10) to be applied, on the basis of multiple measurements of equivalent reflections. The structure was solved by direct methods, developed by successive difference Fourier syntheses, and refined by full-matrix least-squares on all $F^2$ data using SHELXTL, version 6.12. For the organic ligand, one of the carboxylate groups (in *4* position) does not link to the gallium atoms and is terminal. It is statistically delocalized onto two positions with an occupancy factor refined to 45/55 ratio. Hydrogen atoms belonging to the benzene ring and the nonbonded carboxylate group were located using geometric constraints. The final refinement including anisotropic thermal parameters of all non-hydrogen atoms converged to $R_1$ = 0.0308 and $R_2$ = 0.0985. The crystal data are given in Table 1. CIF file is provided in Supporting Information.

**Powder X-ray Diffraction Analysis.** X-ray powder diffraction data of MIL-120 (Ga) were collected on ID31 at ESRF. The beamline receives X-rays from the synchrotron source (which operates with an average energy of 6 GeV and a current beam of typically 100 mA) from an undulator device. The incident X-ray wavelength was 0.79989667 Å using an incident beam size of 2.0 mm (horizontal) × 1.0 mm (vertical). The sample was rapidly spun during data collection to ensure good powder averaging. Extractions of the peak positions, pattern indexing, Fourier calculations, and Rietveld refinements were carried out with the TOPAS[41] program. Unit cell and space group were found unambiguously by the LSI-Indexing method with satisfactory figure of merit [$M_{20}$ = 244] and are similar to those of the aluminum analogue. All the atomic coordinates of the MIL-120 (Al)[35] skeleton were used as the starting model in the Rietveld refinement. At this stage, the $R_{Bragg}$ factor converged to 0.054 and the water molecules exhibited anomalous high thermal parameters. Difference Fourier calculations then revealed an additional water molecule (Ow4) whose occupancy factor was refined in correlation with that of the closest neighboring Ow2. That allowed decreasing significantly the structural model indicator $R_{Bragg}$ and profile factors. Nevertheless, the thermal parameters of the water molecules remained relatively high and have been fixed. This may reflect some additional disorder of the water species within the tunnels. The anisotropic line broadening effect was modeled by using spherical harmonics series. At the final stage, Rietveld refinement involved the following parameters: 28 atomic coordinates, 4 thermal and 3 occupancy factors, 1 scale factor, 1 zero-point, 4 cell parameters, 17 background parameters, and 34 parameters to model the evolution diffraction lines shape. Figure 2 shows the final fit obtained between calculated and observed patterns and corresponds to satisfactory crystal structure model indicator and profile factors (see Table 1).

**Thermogravimetric Analysis.** The TG experiments were carried out on a TA Instruments type 2050 thermoanalyzer TA under oxygen gas flow with a heating rate of 1 °C $min^{-1}$.

**Infrared Spectroscopy.** IR spectra were collected on a Nicolet 550 FTIR spectrometer at room temperature in the range 400−4000 $cm^{-1}$, with samples in potassium bromide pellets.

**Solid-State NMR.** $^{71}$Ga NMR spectra were recorded at an operating frequency of 152.50 MHz on a Bruker AVANCE-500 WB (11.7 T) spectrometer using 2.5 mm zirconia rotors. For 1D rotor-synchronized echo spectra, a two pulses sequence was used and the pulse length was optimized. The length of the first pulse ($\pi$/2) was 2.0 and 1.5 $\mu$s and the length of the second pulse ($\pi$) was 4.0 and 3.0 $\mu$s for the MIL-120 and MIL-124, respectively. The effective radio frequency field $\nu_{RF}$ was 150 kHz for both. The rotor spinning rate $\nu_{Rot}$ was 30 kHz, with a 0.5 s recycle delay. The spectral window was set to 0.5 MHz. For 2D slow-CTMAS spectra, a three pulses sequence was used and the pulse length was optimized. The pulses were selective ($\pi$/2) on the central transition and their length was 5.0 and 3.75 $\mu$s for the MIL-120 and MIL-124, respectively. The radio frequency field $\nu_{RF}$ was 15 kHz for both. The rotor spinning rate $\nu_{Rot}$ was 1000 Hz ± 2 Hz, with a 0.5 s recycle delay. The spectral window was set to 1 MHz. The delay $t_s$ was 30 $\mu$s corresponding to an angle jump of 10.8°. Data acquisitions were performed using 4096 scans per $t_1$ step and the STATES mode.

## Structure Description

**Inorganic Motif.** Both MIL-120 and MIL-124 structures are built up from the same inorganic block consisting of infinite rods of gallium-centered octahedra sharing a common edge (Figure 3). There are two nonequivalent crystallographic sites for the gallium cations (Ga1 and Ga2), which are linked to four hydroxyl bridging groups and two carboxyl oxygen atoms from the organic linker.

(41) *Topas V4.1: General Profile and Structure Analysis Software for Powder Diffraction Data*; Bruker AXS Ltd, 2008.

**Table 1. Crystal Data and Structure Refinement for the Gallium Trimellitate MIL-124 from Single-Crystal and Gallium Pyromellitate MIL-120 from Powder**

| | | |
|---|---|---|
| identification code | MIL-124 (Ga) | MIL-120 (Ga) |
| empirical formula | $Ga_2O_{10}C_9H_8$ | $Ga_4O_{21.6}C_{10}H_{10}$ |
| formula weight | 415.59 g·mol$^{-1}$ | 754.65 g·mol$^{-1}$ |
| temperature | 296(2) K | |
| wavelength (Å) | 0.71073 | 0.79989667 |
| crystal system, space group | monoclinic, $P2_1/n$ | monoclinic, $C2/m$ |
| $a$ (Å) | 7.1517(2) | 9.84786(6) |
| $b$ (Å) | 22.9276(5) | 20.2164(2) |
| $c$ (Å) | 7.6767(1) | 7.62728(5) |
| $\beta$ (°) | 97.649(1) | 133.1981(5) |
| $V$ (Å$^3$) | 1247.56(5) | 1106.98(2) |
| Z, calculated density | 4, 2.213 | 2, 2.264 |
| absorption coefficient | 4.371 mm$^{-1}$ | |
| $F$(000) | 816 | |
| crystal size | 0.22 × 0.10 × 0.02 mm | |
| $\theta$ range for data collection | 1.78 to 30.09° | 3.0 to 46.0° |
| limiting indices | $-10 \le h \le 10$, $-32 \le k \le 32$, $-10 \le l \le 10$ | |
| reflections collected/unique | 78 391/3640 [$R$(int) = 0.0307] | |
| completeness to $\theta$ = 30.06 | 99.7% | |
| absorption correction | semiempirical from equivalents | |
| lmax. and min transmission | 0.9177 and 0.4464 | |
| refinement method | full-matrix least-squares on $F^2$ | |
| data | 3640 | 584 |
| no.structural parameters | 236 | 36 |
| no.non-hydrogen atoms | 24 | 13 |
| GOF on $F^2$ | 1.188 | 1.701 |
| final $R$ indices [$I > 2\sigma(I)$] | $R_1$ = 0.0301, $R_2$ = 0.0953 | |
| $R$ indices (all data) | $R_1$ = 0.0345, $R_2$ = 0.1053 | |
| largest diff. peak and hole | 2.886 and −1.254 e Å$^{-3}$ | |
| no. profile parameters | | 56 |
| $R_P/R_{wp}$ | | 0.094/0.121 |
| $R_{Bragg}$ | | 0.035 |

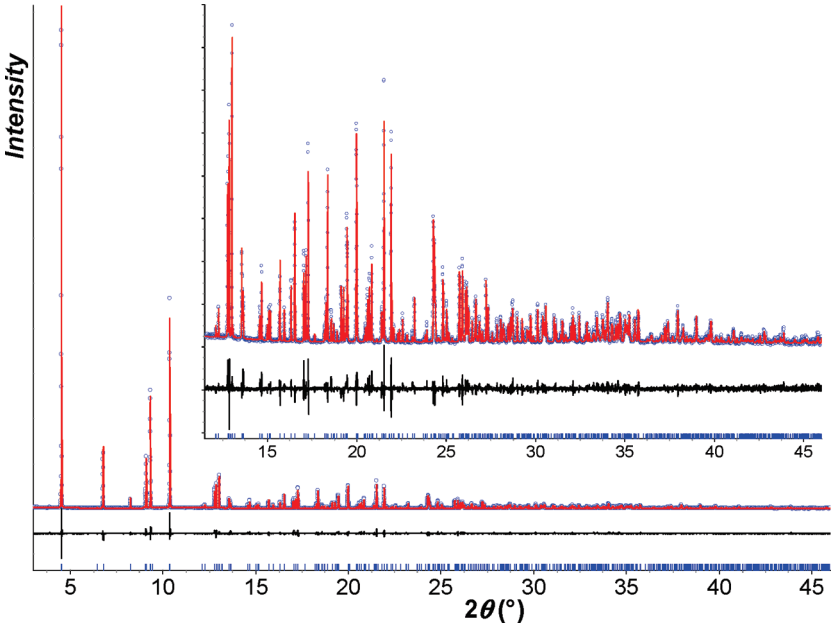


**Figure 2.** Final Rietveld plot of the gallium pyromellitate MIL-120 (X-ray powder data from station ID31 at ESRF, $\lambda$ = 0.79989667 Å, room temperature). Observed data are shown by circles; the calculated pattern is displayed by the red solid line; the lower black curve is a plot of the difference, observed minus calculated.

The occurrence of bridging $\mu_2$-OH ligands is a good agreement with the bond valence calculations[42] with values in the range 0.99−1.15 (expected value for OH = 1.2). The positions of the coordinated species (OH or O) differ for the two types of gallium. Ga1 (in special position *4 g*, 2-fold axis, for MIL-120 and general position *4e* in MIL-124) is surrounded by the two oxo species belonging to the same edge and the remaining four hydroxo species are both on the equatorial and apical positions of the coordination polyhedron. Ga1−O distances are 1.9705(8) and 2.0093(8) Å in MIL-124, and 1.993(7) in MIL-120, whereas Ga1−OH distances range from 1.9293(8) to 2.0172(8) Å in MIL-124, and 1.921(7) and 1.941(4) in MIL-120. The second gallium atom Ga2

(42) Brese, N. E.; O'Keeffe, M. *Acta Crystallogr. B* **1991**, *47*, 192.

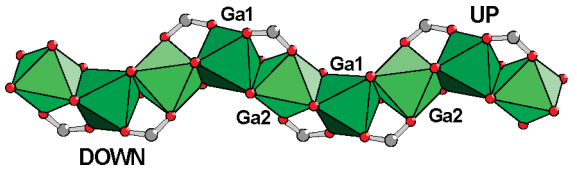


**Figure 3.** Representation of the infinite edge-sharing zigzag chains of gallium-centered octahedral units. *Cis* connection alternates with the trans connection along [10−1] or [102] in MIL-124 and MIL-120, respectively. Dark green: Ga1 octahedron; light green: Ga2 octahedron. Up and down Ga1-centered octahedra correspond to the gallium alternatively pointing upward and downward the axis of the chains.

(in special position *4f*, inversion center, for MIL-120 and general position *4e* in MIL-124) has two oxo species in the apical positions and the remaining four hydroxo species are on the equatorial positions of the coordination polyhedron $GaO_2(OH)_4$. It results in a less distorted octahedral environment for Ga2, compared to Ga1, with Ga2−O distances equal to 1.9858(8) and 2.0052(8) Å in MIL-124, and 1.975(6) in Å MIL-120. The Ga2−OH distances are slightly smaller than those of Ga2−O, with the range 1.9490(8)−1.9733(8) Å in MIL-124 and 1.951(4)−1.951-(7) Å in MIL-120. We observed that the distance amplitude is slightly smaller for Ga2 than Ga1 in both compounds. The gallium cations are linked to each other through a common edge of two $\mu_2$-OH groups with a strict alternation −Ga1−Ga2− sequence. This particular type of connection generates infinite zigzag chains with a cis−trans mode because of the different positions of $\mu_2$-OH within the octahedral surroundings of Ga1 and Ga2. Such inorganic chains are running along the [10−1] and [102] direction in MIL-124 and MIL-120, respectively. Although this specific inorganic motif was found in one of the parent aluminum pyromellitate (MIL-120),[35] it was not reported in other carboxylates involving gallium or other trivalent transition metals. In fact, only straight chains with trans connection mode was observed in solids relating to the frameworks based on corner-sharing octahedral units (see for instance, MIL-53 (Ga),[18−20] MIL-68 (Ga),[21] MIL-61 (Ga)[24] or gallium acetate[23]).

**Structure of MIL-124 ($Ga_2(OH)_4[C_9O_6H_4]$).** In MIL-124, adjacent inorganic chains are linked to each other through the carboxylate functions in *1*,*2* positions of the trimellitate ligand, with a syn−syn bidentate mode bridging the two gallium atoms Ga1 and Ga2. It results in the formation a layer-like network developing in the (*a*,*c*) plane. The third carboxylate function (4 position) of the organic moieties points toward the *b* axis, perpendicularly up and down to the gallium hydroxide trimellitate sheets (Figure 4). This *4*-carboxylate group is delocalized on two equivalent positions (regarding to the *1*,*2* positions of the other carboxylates), giving rise to two distinct crystallographic sites with a population ratio close to 50% (single-crystal XRD analyses gave the ration 45/55). The mixed organic−inorganic layer $Ga_2(OH)_4[C_9O_6H_4]$ is neutral, indicating that the trimellitate moiety is protonated once. Indeed, the third *4*-carboxylate group is not bonded to gallium cations and corresponds to a configuration of carboxylic acid (R-$CO_2$H). The examination of the C−O

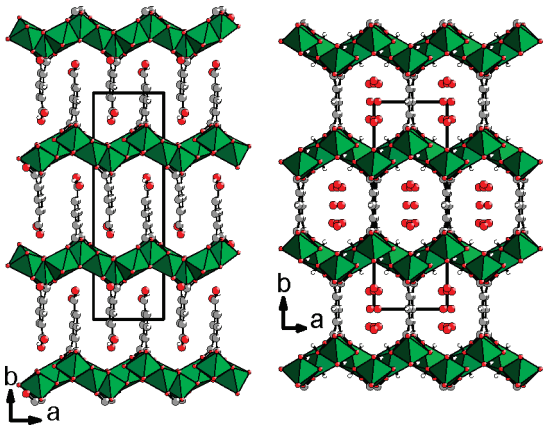


**Figure 4.** Representation of the structures of the gallium trimellitate MIL-124 (left) and gallium pyromellitate MIL-120 (right).

distances did not revealed any clear evidence of such protonated carboxyl oxygen. Only one of the terminal C−O bonding is slightly longer than its neighboring one (C−O = 1.274(3) and 1.276(3) Å for one set of $CO_2$ position; C−O = 1.249(4) and 1.295(5) Å for the second set of $CO_2$). However, infrared spectroscopy showed a strong band at 1716 $cm^{-1}$ reflecting the $\nu_{C-OH}$ vibration (protonated carboxyl oxygen), together with the $\nu_{C-O}$ vibration at 1555 $cm^{-1}$ because of the C−O−M bonding (see Supporting Information S1). The lack of accuracy from the XRD analysis might come from the disorder of this nonbonded carboxylic acid functions and only an average situation is visible with this technique. In this compound, the trimellitate adopts a $\mu_4$-$\eta^1$:$\eta^1$:$\eta^1$:$\eta^1$ connection mode, leaving one nonbonded carboxylate group. The three-dimensional cohesion of the MIL-124 structure is ensured via the existence of the hydrogen bond interactions between the terminal carboxylic acid from one gallium hydroxide trimellitate layer with the bridging hydroxo groups from an adjacent one (Figure 5). Typical hydrogen bond distances are observed between the $\mu_2$-OH and the −$CO_2$H groups (Ga−O2···O10A−C9A = 2.624(2) Å; Ga−O1···H1−O9A−C9A = 2.970(2) Å/Ga−O4···O10B−C9B = 2.772(2) Å; Ga−O4···H12−O10A−C9B = 3.433(1) Å). These mixed organic−inorganic sheets are stacked along the *b* axis, involving the close packing of the trimellitate molecules, which are aligned parallel to each other along the (*b*,*c*) plane. The distance between each aromatic ring is close to 3.8 Å, reflecting weak $\pi-\pi$ interactions and these also strengthen the cohesion of the structure.

**Structure of MIL-120 ($Ga_4(OH)_8[C_{10}O_8H_2]$).** The situation differs significantly in MIL-120 since the tetradentate linker is fully connected to the inorganic chains (Figure 4). Each carboxylate group plays the role of syn−syn bidentate bridge between the gallium atoms Ga1 and Ga2 and the pyromellitate ligand links four distinct chains with the $\mu_8$-$\eta^1$:$\eta^1$:$\eta^1$:$\eta^1$:$\eta^1$:$\eta^1$:$\eta^1$:$\eta^1$ connection mode. In this case, only the vibration band due to the C−O bonding ($\nu_{C-O}$) are observed at 1567 $cm^{-1}$ by infrared spectroscopy (see Supporting Information S2). It results in the generation of one-dimensional channels

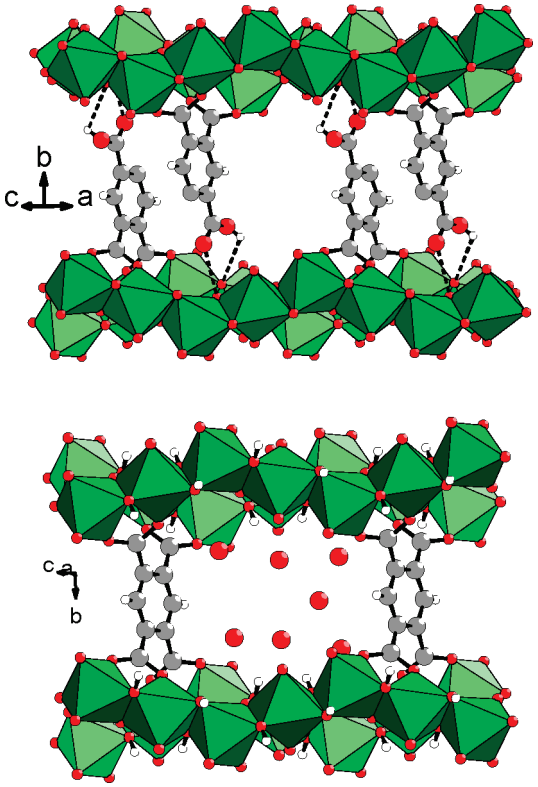


**Figure 5.** Representation of the connection mode of the organic linker in MIL-124 (top) and MIL-120 (bottom).

running along the *c* axis, with calculated pore free diameter of 4.7 × 5.5 Å. These channels are delimited by inorganic chains in the (110) plane and aromatic rings of the pyromellitate linker, aligned perpendicularly to the gallium hydroxide chains and parallel to the (10−1) plane. In MIL-120, the inorganic rods are shifted with $a \approx a/2$ translation, compared to the MIL-124, where they are stacked in order to optimize the close packing along the *b* axis (Figure 5). If one considers the serrated chains with alternation of *up* and *down* Ga1-centered octahedral (Figure 3), the positions along the *b* axis are up−up and down−down in MIL-124 from one chain to another one, whereas they are up−down and down−up in MIL-120. Within the channels are encapsulated water molecules which are statically disordered on several positions. They are interacting via a hydrogen bond network with the hydroxo groups (Ow1···H1−O1 = 2.172(7) Å) and with other water species (Ow1···Ow4 = 2.55(3) Å; Ow1···Ow3 = 2.74(2) Å; Ow2···Ow3 = 2.72(2) Å).

Both compounds have been synthesized at very low pH (0.5−1) with similar acidity constants ($pK_a$ values for trimellitic acid: 2.52, 3.84, and 5.20 and pyromellitic acid: 1.92, 2.87, 4.49 and 5.63). However, in one case, one nonbonded protonated carboxylate is observed (MIL-124) whereas all the carboxylate functions are bonded to the metal atoms (MIL-120). It was found that two adjacent carboxylate groups (positions 1,2 or 4,5) attached to the aromatic ring are able to link two distinct gallium atoms sharing a common $\mu_2$−OH edge from two different chains, but one single carboxylate (position 4) does not in MIL-124.

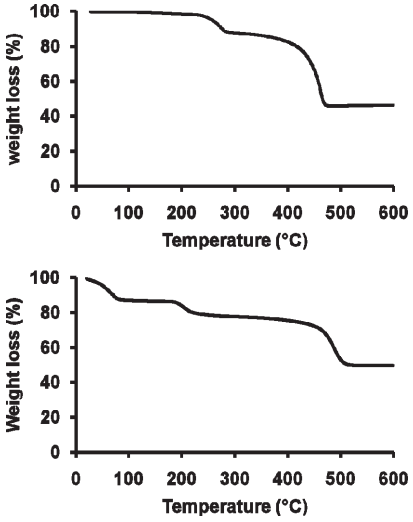


**Figure 6.** Thermogravimetric curves of the gallium trimellitate MIL-124 (top) and the gallium pyromellitate MIL-120 (bottom) (under $O_2$, 1 °C $min^{-1}$).

The possibility of bidentate bridging connection was nevertheless reported in many compounds in MIL-53 (Ga)[18−20] or MIL-68 (Ga),[21] isolated with 1,4-benzenedicarboxylic acid, for instance. For the latter, the inorganic chains are based on the trans-connection of $GaO_6$ octahedra through corners.

**Thermal Analyses.** The thermogravimetric curve (Figure 6) of the gallium trimellitate MIL-124 exhibits two events of weight losses. The first step (11.1%wt) occurs from 220 up to 280 °C and may be assigned to the partial decomposition of the organic ligand with the removal of the nonbonded $CO_2$ species (calcd 10.6%). The second weight loss between 370 and 450 °C, is attributed to the departure of the remaining organic part together with $H_2O$ coming from the dehydroxylation (obs 43.1%; calcd 44.3%). The final plateau from 450 °C corresponds to amorphous gallium oxide ($Ga_2O_3$ obs 45.8%; calcd 45.1%). X-ray thermodiffraction patterns (Supporting Information S3) indicate that MIL-124 is stable up to 280 °C, and then only the first Bragg peak shifted to slightly higher angle (~9° 2$\theta$) is visible but getting broader, and this reflects the loss of crystallinity when increasing the temperature.

The thermogravimetric analysis (Figure 6) of the gallium pyromellitate MIL-120 reveals three steps during the weight loss process. The first event (12.6%) appears from room temperature up to 85 °C and is assigned to the evacuation of the water molecules (~5.3 $H_2O$ per $Ga_4$ unit) from the framework channels. It is followed by two weight losses (9% up to 260 °C and 28.5% up to 520 °C. This might be attributed to the water species coming from the dehydroxylation (−2 $H_2O/Ga_4$; calc: 4.8%) together with a part of the organic ligand (ex $-CO_2$; calcd 5.8%). The third weight loss would correspond to the complete removal of the organic linker. The total calculated weight loss of $2H_2O + H_4$btec is 38.4% and is close to the observed value (9 + 28.5 = 37.5%). Above 520 °C, a plateau corresponding to the gallium oxide residue (obs 49.9%; calcd 49.7%).) is observed. The X-ray thermodiffraction patterns

indicate that the compound is stable up to 260 °C (Supporting Information S4).

**Solid-State NMR using Slow-CTMAS.** X-ray diffraction analyses of the MIL-120 and MIL-124 compounds reveal that both materials exhibit two different crystallographically independent sites of 6-fold coordinated gallium atoms. In the present work, we focused our attention on the use of the slow-CTMAS[40] sequence in order to characterize the gallium sites from the SSNMR point of view. Ga has two active NMR nuclei, $^{69}$Ga (60.5%) and $^{71}$Ga (39.5%), both are quadrupolar with a spin of $I = 3/2$. $^{71}$Ga has higher receptivity and smaller quadrupole moment (i.e., smaller quadrupole coupling constant and narrower line width) than $^{69}$Ga, so $^{71}$Ga is the nucleus of choice for NMR observations in spite of its lower natural abundance. Ga yields broad signals and broad NMR spectra which are often difficult to observe accurately or to interpret structurally.

The NMR investigations (i.e., the counting of the number of crystallographic sites and the extraction of NMR parameters) and high resolution of quadrupolar nuclei can be achieved with static or MAS experiments. For the latter, a wide range of techniques such as ultrahigh speed MAS, rotor-synchronized echo, QPASS[36] (quadrupolar phase adjusted spinning sidebands), MQMAS[37,38] (multiple quantum magic angle spinning), and STMAS[39] (satellite transition magic angle spinning) is available. The QPASS experiment separates spinning sidebands by order in a two-dimensional experiment. The MQMAS and STMAS spectroscopies are respectively based on the correlation of multiple and single quantum and on the correlation of single quantum satellite and central transitions in a two-dimensional experiment. All these techniques require strong RF power and fast spinning speed. In the case of large Ga quadrupolar coupling, routine methods, such as MQMAS and STMAS, can not be used. Indeed, it is impossible to acquire MQMAS and STMAS spectra because of the low efficiency of coherence transfer, even at ultrahigh magnetic fields. The QPASS experience would be generally speaking more suited, but it suffers from the overlap of patterns from multiple sites of different symmetry in a material. In such a case, the rotor-synchronized echo technique, static experiment and nuclear quadrupole resonance (NQR) spectroscopy are preferred.

The MIL-120 and MIL-124 phases have been studied at medium magnetic field (500 MHz $^1$H resonating frequency, 11.7 T) and spectra collected with rotor-synchronized echo sequence were unsuccessful (Figure 7) to resolve the two different types of Ga. Therefore, an alternative approach is required to overcome this limitation. The recently proposed STREAQI/slow-CTMAS[40] method is specifically designed for nuclei with a large quadrupolar coupling. This 2D technique, which is a pseudo-static experiment, correlates two different orientations of the electric field gradient (EFG) tensor. It reminds of the first 2D SSNMR experiment applied in solids, the $^2$D

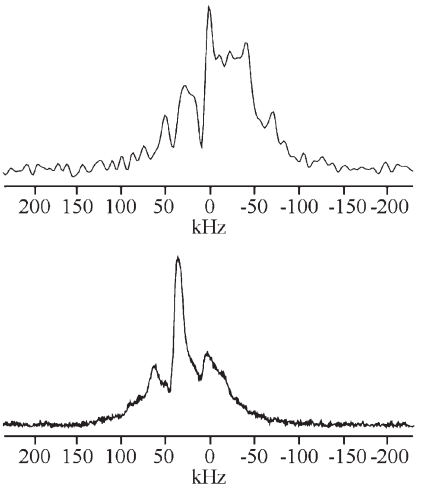


**Figure 7.** $^{71}$Ga rotor-synchronized echo spectra of the gallium trimellitate MIL-120 (top) and MIL-124 (bottom).

tensor reorientation experiment[43] from Spiess, which have been reviewed by Schmidt-Rohr and Spiess.[44] The pulse sequence has just the basic three pulses scheme: the first pulse converts the magnetization along the $z$-axis into a magnetization along the $y$-axis, leaves the magnetization in the plane being chemical shift and quadrupolar coded during $t_1$ evolution. After the second pulse the magnetization is stored along the $z$-axis where a change in orientation takes place with the rotor motion (and not as in the 2D tensor reorientation by the internal motion) and the third pulse brings back the magnetization along the $y$-axis allowing observation of the magnetization during $t_2$ with a different orientation than during the $t_1$ evolution. The main advantages of slow-CTMAS are the use of slow MAS speed and the application of a weak RF excitation. Slow-CTMAS is a selective pulse sequence, which only excites the central transition, and correlates different orientations as ridges of the single quantum-single quantum central transition to central transition correlation. This can be performed using conventional MAS probe hardware. Another advantage, which is considerable, is that the experiment can be achieved at moderate or even low magnetic field. In other words, this technique requires only standard equipment. Therefore the slow-CTMAS experiment seems to be very promising in the evaluation of the NMR parameters: the quadrupole coupling constant ($C_Q$) and the asymmetry parameter ($\eta$). However, it is surprising that slow-CTMAS has not yet attracted much attention from NMR spectroscopists. Indeed, since its publication in 2007,[40] no experimental slow-CTMAS spectrum have been published in the literature. Undoubtedly, one reason for this is that it is difficult to extract the NMR parameters from experimental spectra. We have examined in detail (experimentally, see Supporting Information S5, and by simulations) the slow-CTMAS approach and we have validated it. We have also developed two methods to extract the NMR parameters ($C_Q$ and $\eta$). In this work we have applied the

(43) Schmidt, C.; Blümich, B.; Spiess, H. W. *J. Magn. Reson.* **1988**, *79*, 269.

(44) Schmidt-Rohr, K.; Spiess, H. W. *Multidimensional Solid State NMR and Polymers*; Academic Press: London, 1994.

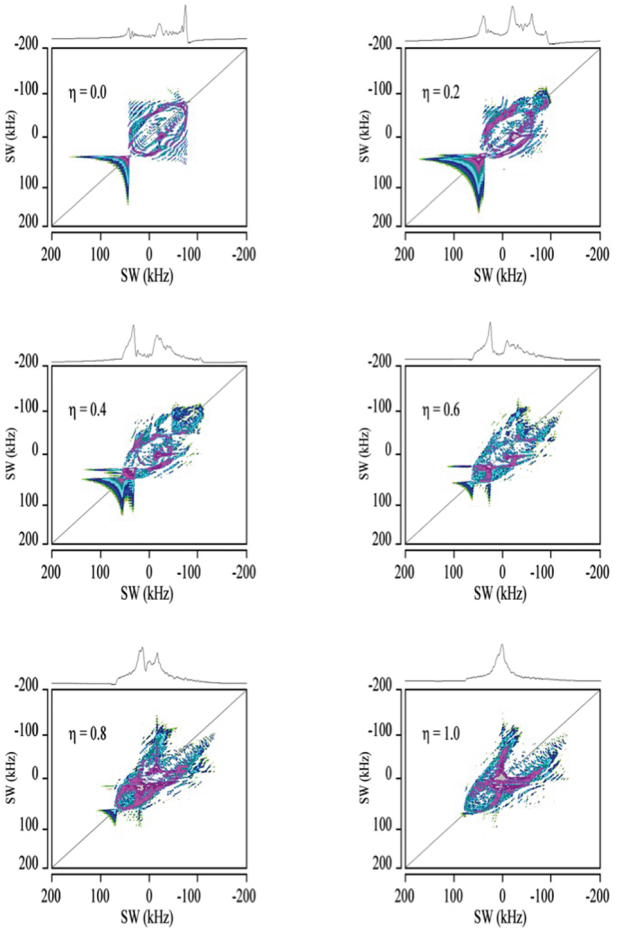


**Figure 8.** $^{71}$Ga 2D slow-CTMAS NMR spectra, simulated by SIMPSON with $\nu_{71Ga}$ = 183.488 MHz ($\nu_{1H}$ = 600 MHz), $C_Q$ = 13 MHz, $\nu_{Rot}$ = 300 Hz, $\omega_{RF}$ = 10 kHz, an angle = 10.8° ($t_s$ = 100 $\mu$s). The acquisitions were performed in the STATES mode. Spectra were calculated using 4180 crystal orientations and 20 $\gamma$ angles. The maximum time step over which the Hamiltonian was considered time independent was 0.5 $\mu$s. 128 points were used in both $t_1$ and $t_2$ dimension.

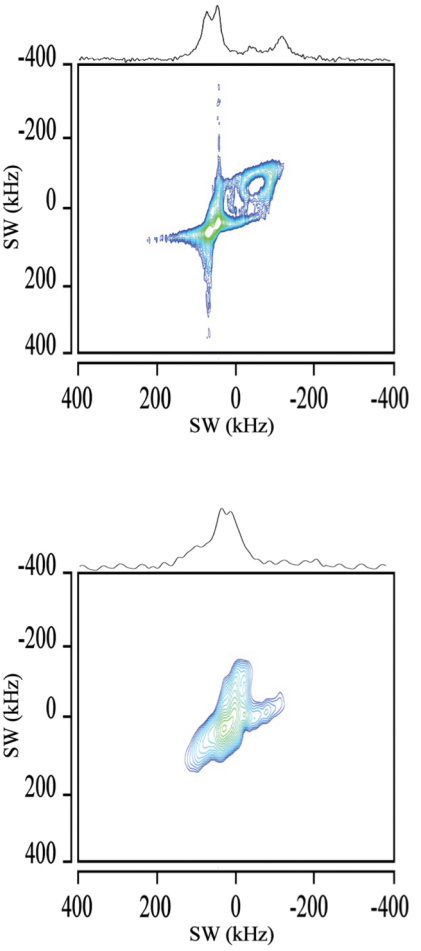


**Figure 9.** $^{71}$Ga 2D slow-CTMAS NMR spectra of the gallium trimellitate MIL-120 (top) and the gallium pyromellitate MIL-124 (bottom).

slow-CTMAS experiment in order to confirm or to invalidate the presence of six-coordinated Ga atoms in the MIL-120 and MIL-124 materials.

Our goal is to extract the NMR parameters ($C_Q$ and $\eta$) from 2D slow-CTMAS spectra and as mentioned above, we have developed two methods to achieve this extraction. The first one is based on simulations using the package SIMPSON:[45] A General Simulation Program for Solid-State NMR Spectroscopy. This "virtual" spectrometer is a powerful tool and is widely used in both liquid and solid state NMR spectroscopy. SIMPSON simulations are made via a Tcl scripting code. We have successfully implemented a script that simulates 2D slow-CTMAS spectra of powders (Figure 8). These spectra exhibit characteristic ridges and their shape takes on a character determined by the asymmetry parameter $\eta$. This method works very well, but unfortunately, it is well-known that such simulations take up too much computational time (several hours). To overcome the drawback of the simulation approach, we propose a second method for extracting NMR parameters. The method is based on the use of singularities and shoulders present in the spectra: from the frequencies at these particular positions, NMR parameters can be computed. In this work, we applied this approach to the MIL-120 and MIL-124 materials.

The $^{71}$Ga 2D slow-CTMAS NMR spectra of MIL-120 and MIL-124 are shown in Figure 9. This discontinuities approach put the emphasis on the highest intensities discontinuities in the 1D spectrum that translates into the most intense ridges in the slow-CTMAS experiment. When the ridges cross the diagonal of the correlation they allow locating the exact positions of a pair of most intense discontinuities in the single quantum spectrum. Two different situations can be observed depending on the value of $\eta$ ($0 \leq \eta \leq 1/3$ and $1/3 \leq \eta \leq 1$) as previously exposed. The following expressions have been expressed by Stauss[46] for quadrupolar interaction alone and by Baugher et al.[47] for quadrupolar and CSA. Once transposed to actual notations with $C_Q$ the quadrupolar interaction $\nu_0$ is the Larmor frequency. The frequencies of discontinuities are listed in Table 2.

(45) Bak, M.; Rasmussen, J. T.; Nielsen, N. C. *J. Magn. Reson.* **2000**, *147*, 296.

(46) Stauss, G. H. *J. Chem. Phys.* **1964**, *40*, 1988.
(47) Baugher, J. F.; Taylor, P. C.; Oja, T.; Bray, P. J. *J. Chem. Phys.* **1969**, *50*, 4914.

**Table 2. Frequencies of Discontinuities**

| | discontinuities | | | | | |
|---|---|---|---|---|---|---|
| $0 \le \eta \le 1/3$ | $\nu_1 = \frac{C_Q^2(3+\eta)^2}{192\nu_0}$ | $\nu_2 = \frac{C_Q^2(3-\eta)^2}{192\nu_0}$ | | $\nu_4 = \frac{C_Q^2\eta^2}{48\nu_0}$ | $\nu_5 = -\frac{C_Q^2(1-\eta)}{12\nu_0}$ | $\nu_6 = -\frac{C_Q^2(1+\eta)}{12\nu_0}$ |
| $1/3 \le \eta \le 1$ | $\nu_1 = \frac{C_Q^2(3+\eta)^2}{192\nu_0}$ | $\nu_2 = \frac{C_Q^2(3-\eta)^2}{192\nu_0}$ | $\nu_3 = \frac{C_Q^2(1-\eta^2)}{24\nu_0}$ | $\nu_4 = \frac{C_Q^2\eta^2}{48\nu_0}$ | $\nu_5 = -\frac{C_Q^2(1-\eta)}{12\nu_0}$ | $\nu_6 = -\frac{C_Q^2(1+\eta)}{12\nu_0}$ |

Inspection of the ridges allows determining which are the discontinuities relevant to the spectrum. The most intense discontinuities, ($\nu_2$, $\nu_5$ for $0 \le \eta \le 1/3$, $\nu_3$, $\nu_5$ for $\eta \le 1/3$) are the most probable, but this not always the case. However, with the SQ projection it is easy to determine which ridge is which. The MIL-120 spectrum exhibits four shoulders and singularities at 56, 34, −30, and −93 kHz. A careful examination of these values, according to the frequencies $\nu_1$, $\nu_2$, $\nu_3$, $\nu_4$, $\nu_5$, and $\nu_6$, shows that they form two pairs of ridges with $P_{1,\nu}$ ($\nu_2 = 53$ kHz ; $\nu_5 = -93$ kHz) and $P_{2,\nu}$ ($\nu_1 = 34$ kHz ; $\nu_5 = -30$ kHz). Using $P_{1,\nu}$ and $P_{2,\nu}$, we obtained two pairs of $C_Q$ frequency and asymmetry parameter $\eta$: $P_{1,(C_Q,\eta)}$ ($C_Q = 14.3$ MHz; $\eta = 0.17$) and $P_{2,(C_Q,\eta)}$ ($C_Q = 9.4$ MHz; $\eta = 0.37$) that correspond to two different environments. The observed difference in $C_Q$ is predicted, and it is because of the distortion in the octahedral environment. Thus, it becomes obvious that $P_{1,(CQ,\eta)}$ and $P_{2,(CQ,\eta)}$ correspond to Ga1 and Ga2 (less distorted) sites, respectively.

The MIL-124 spectrum exhibits three shoulders at 4, 28, and 106 kHz, related to $\nu_3$, $\nu_2$, and $\nu_1$. The latter is the end of the correlation ellipse. In the same way, an examination of these frequencies shows that they form only one ensemble of frequencies. The extracted parameters are $C_Q = 14.1$ MHz and $\eta = 0.94$. In other words, only one site is observed. Several spectra (not shown here) have been recorded by changing either the center of the irradiation or slow-CTMAS delay $t_s$ (in the range of 6.7 and 42 $\mu$s, corresponding to an angle of jump in the range of 2.4 and 15°). The result obtained are still the same, only one crystallographic site is detected. One must notice that a disordered occupancy of one carboxylate arms of trimellitate linker is observed by X-ray diffraction. This is compatible with a possible motion in MIL-124 of the incompletely connected organic linker. Such a motion, which would cause a strong broadening in spectra beyond observation is known in NMR spectroscopy of solids and has been discussed by Ashbrook and Wimperis[48] in STMAS/MQMAS experiments. Indeed, unlike in MIL-120, the tridentate linker is not fully connected to the inorganic chains in MIL-124 (Figure 5). Oscillations of linkers which are half connected, would have a motional time scale faster than the slow-CTMAS delay $t_s$. It would result in local modulation of the electron density of neighboring gallium atoms, described as disorder. To overcome this limitation, two strategies might be furthered: cooling down the sample to freeze the possible motion, or perform a geometry optimization and select those geometries that would reproduce accurately the experimental values of the observed site, and infer a good estimate of the quadrupolar parameters of the unobserved one. Both approaches can not be performed yet, for technical reasons for variable temperature NMR and for the too large amount of computer resources needed for this study.

(48) Ashbrook, S.; Wimperis, S. *Prog. Nucl. Magn. Reson. Spectrosc.* **2004**, *45*, 53.

## Conclusion

In this study, two new members of gallium-based MOF compounds have been isolated from hydrothermal reactions and characterized by X-ray diffraction analyses and $^{71}$Ga SSNMR spectroscopy. By using either pyromellitate (MIL-120) or trimellitate ligands (MIL-124), a structure based on the connection of edge-sharing octahedral $GaO_6$ generating infinite chains have been observed; gallium atoms occupy two distinct crystallographic sites in both compounds. Depending on the number of carboxylate functions, a three-dimensional framework (MIL-120) or layered network (MIL-124) is formed. In the latter, one of the carboxylate arm is not bonded and remains free on two distinct crystallographic positions. To detect the two gallium sites from SSNMR, we have employed the slow-CTMAS method. We have shown that it can be usefully implemented and pushes the limit of detection of large quadrupolar nuclei even further than the most successful methods like MQMAS and STMAS, using only classical MAS probes, low radio frequency field and low magnetic fields. This method should meet larger uses because it is less technically demanding even if some processing efforts should be added to get a full routine analytic method. In this specific study it has been demonstrated two facts: (1) SSNMR spectroscopy confirms the presence of two different crystallographic Ga sites in the MIL-120 material and validate the structure model, and (2) for MIL-124, one site is observed and with slow-CTMAS the second site of the structure can not be detected, indicating most probably a motion of the half connected linker.

**Acknowledgment.** The authors would like to thank Dr Eric Leroy and Dr Michel Latroche (ICMPE, UMR CNRS 7182, Thiais, France) for their assistance for the SEM images.

**Supporting Information Available:** CIF files, Figures S1−S2 (IR spectra), S3−S4 (X-ray thermodiffraction patterns), and S5 ($^{79}$Br slow-CTMAS NMR spectra of L-tyrosine hydrobromide). This material is available free of charge via the Internet at http://pubs.acs.org.